


Engineering Resonance Modes for Enhanced Magnetolectric Coupling in Bilayer Laminate Composites for Energy Harvesting Applications

Atal Bihari Swain[✉], S. Dinesh Kumar, Venkatachalam Subramanian, and Pattukkannu Murugavel^{✉*}
Department of Physics, Indian Institute of Technology Madras, Chennai 600036, India

 (Received 12 August 2019; revised manuscript received 9 December 2019; accepted 24 January 2020; published 11 February 2020)

The magnetolectric (ME) effect in composites, a strain-mediated coupling phenomenon between piezoelectric and magnetostrictive phases, has a wide range of technological applications. Here, ME coupling phenomena are explored in Pb-free piezoelectric, $0.5\text{Ba}(\text{Zr}_{0.2}\text{Ti}_{0.8})\text{O}_3$ - $0.5(\text{Ba}_{0.7}\text{Ca}_{0.3})\text{TiO}_3$ and piezomagnetic NiFe_2O_4 bilayer laminate composites. The direct and converse ME coupling strengths are found to be enhanced at the electromechanical resonance modes, rather than at the off-resonance frequencies. Here, it is proposed to further enhance the ME coupling strength at electromechanical resonance modes by the in-phase superimposition of the radial and second bending modes via varying the bilayer thickness, which, in turn, varies the volume fraction of the bilayer. The proposed enhanced ME coupling is experimentally demonstrated at a theoretically envisaged bilayer thickness of about 1.8 mm. This results in a large direct ME coupling coefficient of $22.5 \text{ V cm}^{-1} \text{ Oe}^{-1}$, which is around 100% more than the values observed at individual resonance modes. The results are further validated by calculations from theoretical models. The method adopted in this work gives a roadmap to the significant enhancement of the ME effect in laminate composites.

DOI: [10.1103/PhysRevApplied.13.024026](https://doi.org/10.1103/PhysRevApplied.13.024026)

I. INTRODUCTION

The ever-increasing demand for alternative energy necessitates the search for energy harvesting from numerous possible resources. Although research into photovoltaic and fuel cells dominates, tapping the energy from other unconsumed energy resources is also an attractive area of research. In this context, piezoelectric ceramics are considered as energy harvesting materials due to their ability to convert energy from a wide range of sources, such as mechanical vibrations, light, and temperature [1,2]. Interestingly, magnetolectric (ME) materials, which are the combination of magnetic and piezoelectric phases, can harvest energy from stray magnetic fields that originate from electric power lines or electronic devices through ME coupling [1–5]. In this way, self-powered electronic devices, requiring low power consumption, can function by harvesting energy from these environmental sources. Typically, these devices operate at resonance modes, where the maximum energy harvesting is achieved when the frequency of the energy source matches that of the device frequency [6]. Although most of these environmental energy sources are in the low-frequency range (10–60 Hz) [7], energy harvesting from sources related to radiofrequency is also equally important for applications in the wireless powering of small

electronic devices [8,9]. Hence, the ME effect is another exciting area of research in the context of the search for alternative energy. Generally, ME effects are envisaged in various materials with geometries prominently in a single phase, particulate composites, and laminated composites. Other than laminate composites, most of these geometries reveal ME coupling either at low temperatures or with low strength, which renders them unsuitable for room-temperature practical applications [10–12]. Better ME coupling is an essential requirement for efficient energy harvesting from ME materials. In this regard, the ME laminate composites, where strong ME coupling can be achieved via an effective strain transfer between constituent phases, could be a potential candidate for energy harvesting [10–12].

In laminate composites, apart from the properties of the constituent ferroelectric and magnetic phases, the quality interface between them determines the strength of ME coupling [13–16]. There are numerous studies where ME coupling is demonstrated to be enhanced by controlling the effective strain transfer across the interface [13–18]. The choice of a suitable buffer layer between the composite layers is an example where the resultant coherent interface in the heterostructure leads to an effective strain transfer [13,15]. It is also demonstrated that the fabrication of multilayers increases the strain from each layer and eventually results in strong coupling [14, 18,19]. Interestingly, an improvement in strain transfer is

*muruga@iitm.ac.in

obtained by having intermediate antiferromagnetic interface layers via exchange bias interactions between the magnetic interfaces [20]. Localized thermal treatment by laser annealing, which induces better crystallinity without damaging the interface, is also demonstrated in the literature [21]. Additionally, the growth of the oriented piezoelectric layer in the lead zirconate titanate (PZT)/Ni heterostructure is observed to yield better ME coupling [22]. Also, the role of anisotropy and the tuning behavior over large ME coupling is reported in the Ni/0.5Ba(Zr_{0.2}Ti_{0.8})O₃ – 0.5(Ba_{0.7}Ca_{0.3})TiO₃ (BZT-BCT)/Ni laminate structure [23]. Furthermore, recently, the enhancement of magnetic energy harvesting in the ME laminate structure by tailoring the geometry of the laminate was reported [5]. Subsequently, a theoretical understanding of the ME effect and its enhancement at the resonant frequency were proposed and demonstrated experimentally in the literature [24–28]. The enhanced ME voltage coefficient is determined to be controlled by the thickness ratio of the piezoelectric and piezomagnetic heterostructure [24]. Also, the enhancement of the ME voltage coefficient is proposed by varying the permeability of magnetic materials [26].

Importantly, ME studies at the natural frequency of the piezoelectric or piezomagnetic material show a massive improvement in ME coupling strength due to a larger strain transfer (100 times) than that of its off-resonance frequency [26–28]. Notably, excitation and frequencies of the natural resonance modes are decided by the geometrical shape and size of the materials [25,28]. The disk-shaped sample shows a radial mode, and two disks bonded together will show bending modes in a bilayer structure [10,27,28]. Although there are reports on the ME effects observed at resonance [26–30], the method of achieving enhanced ME effects by tuning the resonance modes is not being investigated.

Here, the method of tuning the radial and bending modes for their in-phase superimposition is adopted in a bilayer laminate composite structure for achieving a vast improvement in ME coupling strength. For this study, Pb-free nontoxic piezoelectric BZT-BCT and soft ferromagnetic NiFe₂O₄ (NFO) with a large piezocoefficient, $d_{33} \sim 620$ pC N⁻¹, and magnetostriction coefficient, $\lambda \sim -33$ ppm, are chosen as the constituent layers for the bilayer laminate composite structure [12,31]. The bilayer laminate composite for an optimized piezoelectric phase thickness reveals a remarkable enhancement in ME effect with maximum direct ME and converse ME coupling coefficients of 22.5 V cm⁻¹ Oe⁻¹ and 25.15 mGcm V⁻¹, respectively, due to the in-phase superimposition of the radial and second bending modes. The voltage generated from the ME composite structure through magnetic energy harvesting is demonstrated to power a series of light-emitting diodes (LEDs). Detailed studies are presented in this work.

II. EXPERIMENTAL METHODS

A. Sample preparation

The morphotropic phase-boundary composition of BZT-BCT is prepared using a conventional solid-state method. A stoichiometric mixture of initial precursors BaCO₃ (purity $\geq 99.9\%$), TiO₂ (purity $\geq 99.9\%$), BaZrO₃ (purity $\geq 99.9\%$), and CaCO₃ (purity $\geq 99.9\%$) are calcined at 1350 °C for 4 h. The calcined powder is pressed into 12 mm pellets after adding 6 wt % polyvinyl alcohol (PVA) as a binder. The green pellets are sintered at 1450 °C for 4 h with an intermittent dwell time of 1 h at 600 °C for PVA evaporation [32]. The NFO is synthesized using NiO and Fe₂O₃ as precursors and calcined at 1200 °C for 12 h. The calcined NFO powder is pressed into 12 mm pellets after adding 6 wt % PVA as a binder. The NFO green pellets are sintered at 1350 °C for 4 h.

B. Experimental methods

The samples are examined for their structure and phase purity by means of x-ray diffraction (XRD) measurements using a Rigaku pro x-ray diffractometer. Silver contacts are made on both sides of the BZT-BCT pellets as electrodes for the ferroelectric measurements by employing a Radiant Technologies Inc. (RT6000S USA) ferroelectric loop tracer. To prepare the bilayer laminate composite, piezomagnetic NFO is covered with Ag on the curved and one of the flat surfaces of the pellet to act as electrodes for poling the piezoelectric layer in the composite. The bilayer laminate composites are made by bonding BZT-BCT and NFO (Ag-painted) layers using silver conducting epoxy (Alfa Aeser) and annealing them at 150 °C for 15 min followed by 200 °C for 30 min to ensure better bonding. Three samples of bilayer composites are made by keeping a NFO thickness of 1.0 mm and varying the BZT-BCT layer thickness to 0.4, 0.6, 0.8, and 1.0 mm. The piezocoefficient is tested using a d_{33} Piezo test meter after poling the sample at 4 kV mm⁻¹ field under ambient temperature for 1 h. A numeric impedance analyzer is employed for the identification of various resonance modes of the bilayer composites. The ME measurement is carried out in longitudinally magnetized and transversely polarized (L-T) mode configuration (using the homemade test measurement unit with lock-in amplifiers SR 830 (for the low-frequency range, 1 mHz–102 kHz) and SR 844 (for the high-frequency range, 25–200 MHz) [28].

III. RESULTS AND DISCUSSION

A. Structural studies

To confirm the phase purity of the synthesized BZT-BCT and NFO compounds, powder XRD is performed at room temperature. The XRD patterns are recorded on BZT-BCT and NFO in powder forms, which are made by crushing sintered pellets. The XRD patterns are shown

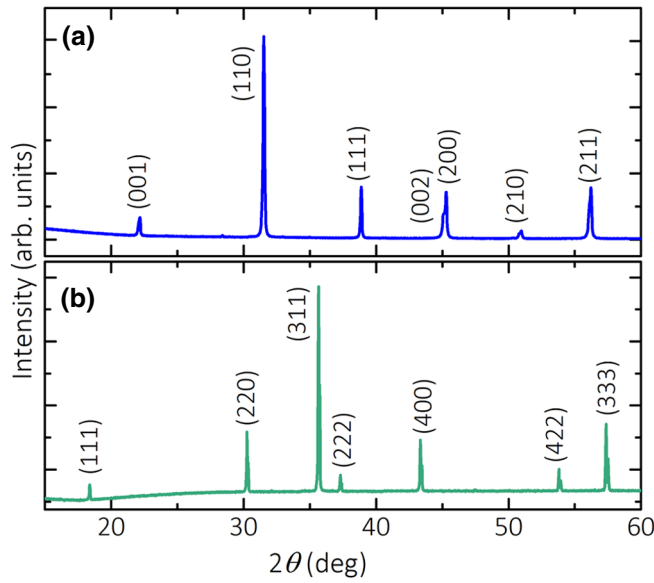


FIG. 1. XRD patterns for (a) BZT-BCT and (b) NFO samples.

in Figs. 1(a) and 1(b), respectively. The XRD pattern for the BZT-BCT sample exhibits perovskite crystal symmetry without any secondary phase. The peaks are indexed to the tetragonal symmetry of the BZT-BCT compound. Similarly, the XRD pattern of NFO confirms the inverse spinel structure without any secondary phase.

B. Resonance modes of a bilayer laminate composite

The efficiency of piezoceramics in piezomechanical devices can be enhanced when operating at piezomechanical resonant frequencies [26–29]. The ME coupling strength will be higher when an ac magnetic field (H_{ac}) is applied at the acoustic resonance modes of the bilayer laminate structure. So, it is necessary to extract the resonance frequencies to achieve better piezoelectric properties. In this regard, the frequency-dependent impedance characteristics of the piezoelectric sample can be used as a tool to obtain details about the resonance modes. The asymmetric bilayer laminate structure generally yields two types of acoustic modes, such as the radial modes at frequencies f_{Rn} and bending modes at the frequencies f_{Bn} , where n is the order of oscillation. In radial modes, the vibrations are in the plane of the structure, and in bending modes the vibrations are out of the radial plane, i.e., along the thickness of the sample [27,28]. Each oscillation mode has a resonance frequency (f_r) followed by an antiresonance frequency (f_a). At f_r , the impedance is minimum with maximum oscillation amplitude, and at f_a the impedance is maximum with minimum oscillation amplitude [29].

The impedance and phase versus frequency plots for the bilayer laminate composite with 0.4-mm thick BZT-BCT and 1.0-mm thick NFO layers (labeled as 0.4BZT-BCT/NFO) are shown in Fig. 2. The labels f_{B1} , f_{B2} , and

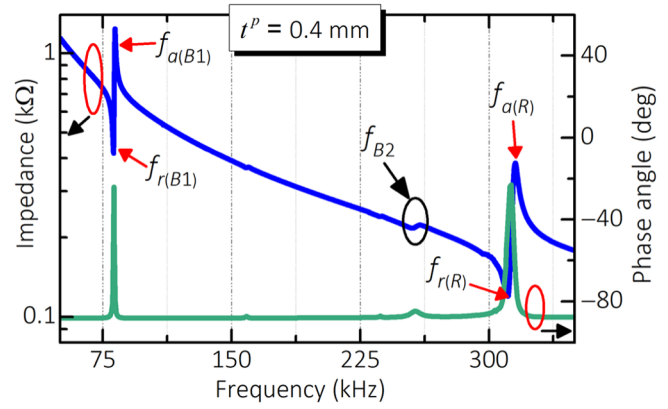


FIG. 2. Impedance and phase versus frequency plots for the 0.4BZT-BCT/NFO laminate composite.

f_R marked Fig. 2 are the first bending, second bending, and radial modes, respectively. The corresponding f_r and f_a for the bending and radial modes are also indicated by arrows in Fig. 2. The frequency of the radial mode, f_r , for a disk-shaped piezoelectric structure is determined by the physical properties and geometrical size of the materials and is defined by

$$f_R = \frac{\beta}{2\pi R} \sqrt{\frac{Y}{\rho(1-\nu^2)}}, \quad (1)$$

where $\rho = [(\rho_m t^m + \rho_p t^p)/(t^m + t^p)]$ and $Y = [(Y_m t^m + Y_p t^p)/(t^m + t^p)]$ are the effective mass density and effective Young's modulus of the bilayer structure, respectively. ρ_m , ρ_p ; t^m , t^p ; and Y_m , Y_p are the densities, thicknesses, and Young's moduli of magnetostrictive and piezoelectric phases, respectively [27]. ν is the effective Poisson ratio of the bilayer structure, and β is the coefficient corresponding to the fundamental radial mode of the bilayer disk of radius R . On the other hand, after bonding the piezoelectric layer with a magnetic layer, constraint due to asymmetric bilayer gives bending modes, the frequencies of which are defined by

$$f_{Bn} = \alpha_n \frac{b}{2\pi R^2} \sqrt{\frac{Y}{12\rho(1-\nu^2)}}, \quad (2)$$

where α_n is the bending mode coefficient, n is the order of bending modes, and $b = t^m + t^p$ is the thickness of the bilayer [27]. It is worth noting that f_R is inversely proportional to the radius of the disk, and f_{Bn} varies with both the thickness and the radius of the composite. Hence, it allows engineering of these radial and bending modes for superimposition by tuning R or b of the bilayer to maximize mechanical vibration in the bilayer disk. This, in turn, may help to improve the strain-mediated ME coupling in the bilayer structure at that frequency. In addition, it gives

an insight into the effect of the volume fraction of piezoelectric layer (V) on the strain-mediated ME coupling. V is defined as $V = [V_p / (V_p + V_m)]$, where V_p and V_m are the volumes of the piezoelectric and magnetostrictive phases, respectively [25,26].

C. Engineering of resonance modes of the bilayer laminate composite

An enhanced ME effect can be envisaged at frequencies where the acoustic modes are made to superimpose. A schematic diagram depicting engineering of the acoustic modes by tuning parameters R and b are represented in Fig. 3.

The diagram in Fig. 3(a) shows the representation of well-separated radial and bending mode oscillations as a function of frequency. Upon varying R and/or b , the bending and radial modes move towards each other, as depicted in Fig. 3(b). At particular R and/or b values, these two modes superimpose at a frequency either in-phase or out-of-phase with each other, as shown in Figs. 3(c) and 3(d), respectively. The out-of-phase superimposition gives a wide frequency bandwidth for ME measurements, but with low ME coupling coefficients [33,34]. However, the in-phase superimposition can enhance ME coupling over a narrow bandwidth region, as shown in Fig. 3(d).

The 0.4BZT-BCT/NFO bilayer laminate composite displays f_{B1} and f_{B2} near 75 and 258 kHz, respectively, along with f_R around 311 kHz, as shown in Fig. 2. Hence, it is possible to tune f_{B2} towards f_R by increasing the thickness of the piezoelectric layer for a particular magnetostrictive layer thickness and thereby make it in-phase superimposition with f_R , to achieve enhanced ME coupling coefficients in the bilayer composite structure.

D. In-phase superimposition of radial and bending modes

The condition to manipulate the superimposition of the radial and bending modes in a bilayer laminate composite

obtained by equating Eqs. (1) and (2) is given by

$$\frac{b}{R} = \sqrt{12} \left(\frac{\beta}{\alpha_n} \right). \quad (3)$$

To estimate the approximate range of b for a particular R value, reported β , α_1 , and α_2 data [27] for the PZT/Ni laminate structure are considered. Consequently, the first-hand calculation from Eq. (3) suggests that the approximate bilayer thickness, b , needs to be about 1.5–2.25 mm, when R is in the 4–6 mm range to obtain the superimposition of the second bending mode with the radial mode of an asymmetric bilayer structure. To tune the resonance modes, bilayer composites with higher t^p , such as 0.6, 0.8, and 1.0 mm, are prepared by keeping t^m of NFO at 1.0 mm and thereby maintaining b around the abovementioned range. Notably, the radius of the bilayer is 5.6 mm. To identify the resonance modes of the bilayer composites, the impedance and phase variations as a function of frequency for all samples are recorded and plotted in Fig. 4.

It is observed that f_{B2} , which is near 258 kHz for the $t^p = 0.4$ mm composite, is shifting towards f_R with a further increase in the value of t^p [0.6 mm; Figs. 4(a) and 4(b)]. Significantly, the $t^p = 0.8$ mm composite shows the superimposition of f_{B2} with f_R at a particular frequency, as shown in Fig. 4(c). For clarity, the enlarged version of the particular region in the impedance plot is shown as an inset in Fig. 4(c). Importantly, the observed identical variation of phase vibration for f_R and f_{B2} in the $t^p = 0.8$ mm composite suggests the in-phase superimposition of these modes, which further elucidates the possibility of strong electromechanical coupling in the structure measured at that frequency. However, the $t^p = 1$ mm composite exhibits the separation of these modes, as displayed in Fig. 4(d) and the respective inset. To confirm the observed in-phase superimposition condition, the expected b value for the disk of particular R is calculated based on the following parameters. The measured densities, ρ_p and ρ_m , of the BZT-BCT and NFO compounds are 5.55 and 4.80 g cm⁻³, respectively. These values are obtained by considering

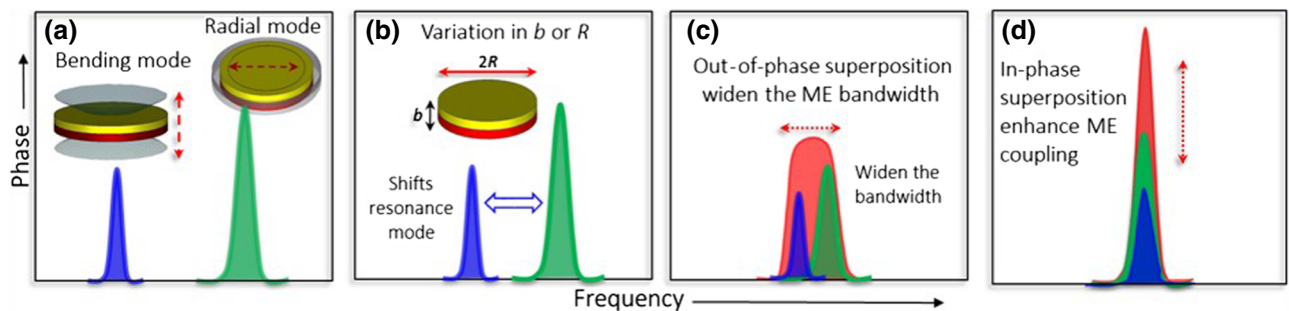


FIG. 3. (a) Schematic representation of radial and bending modes of the bilayer laminate structure. (b) Change in positions of radial and bending modes caused by variation in R and/or b . (c) Out-of-phase superimposition and (d) in-phase superimposition of the modes.

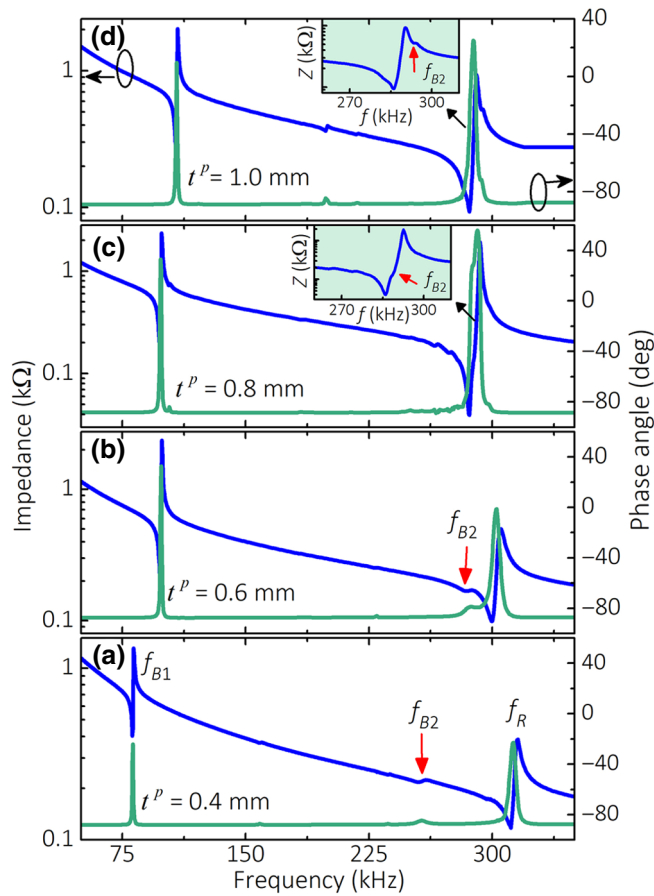


FIG. 4. Impedance and phase as a function of frequency for $t^p = 0.4, 0.6, 0.8,$ and 1.0 mm in the BZT-BCT/NFO laminate structure. Insets show enlarged versions of the impedance plots near the region where the modes are merging.

$Y = 11378.5 \text{ N m}^{-2}$ and $\nu = 0.36$, with reference to values of Y_p , Y_m , and ν reported in the literature [35,36]. Subsequently, the obtained bending and radial mode constants α_1 , α_2 , and β of the BZT-BCT/NFO bilayer from Eqs. (1) and (2) are 6.38, 18.80, and 1.85, respectively. On substituting them into Eq. (3), the value of b calculated for the superimposition of modes in the bilayer composite is 1.77 mm. This value is in accordance with the value (1.8 mm) used in the experiment, which resulted in the superimposition of the modes, as shown in Fig. 4(c). Therefore, the resonance effect on ME coupling and the expected enhancement at a superimposed frequency can be better understood from the ME characteristics of these laminate structures measured at off-resonance and resonance frequencies.

E. Magnetolectric studies at the off-resonance frequency

The direct ME (DME) effect of the laminate composites are characterized at 1 Oe H_{ac} field with 1 kHz

off-resonance frequency. The measured DME voltage coefficient (α_{DME}) as a function of the dc magnetic field (H_{dc}) for the composites with various t^p are shown in Fig. 5(a). The plots display typical behavior of α_{DME} with respect to H_{dc} [12–14], where α_{DME} increases with H_{dc} before reaching a maximum near 145 Oe, and thereafter shows a decreasing trend for higher H_{dc} values. The maximum $\alpha_{\text{DME}} = 124 \text{ mV cm}^{-1} \text{ Oe}^{-1}$ is observed for the $t^p = 0.6$ mm composite. Similarly, the converse ME (CME) measurements of the bilayer laminate composite are performed by applying a peak-to-peak voltage (V_{pp}) of 5 V at 1 kHz. The measured CME coefficient (α_{CME}) as a function of H_{dc} for the composites are plotted in Fig. 5(b). The plots show similar behavior to that of α_{DME} , with a maximum value observed near 145 Oe. The maximum α_{CME} value of $78 \mu\text{Gcm V}^{-1}$ is observed for the $t^p = 1.0$ mm composite due to the higher BZT-BCT volume fraction. Variations

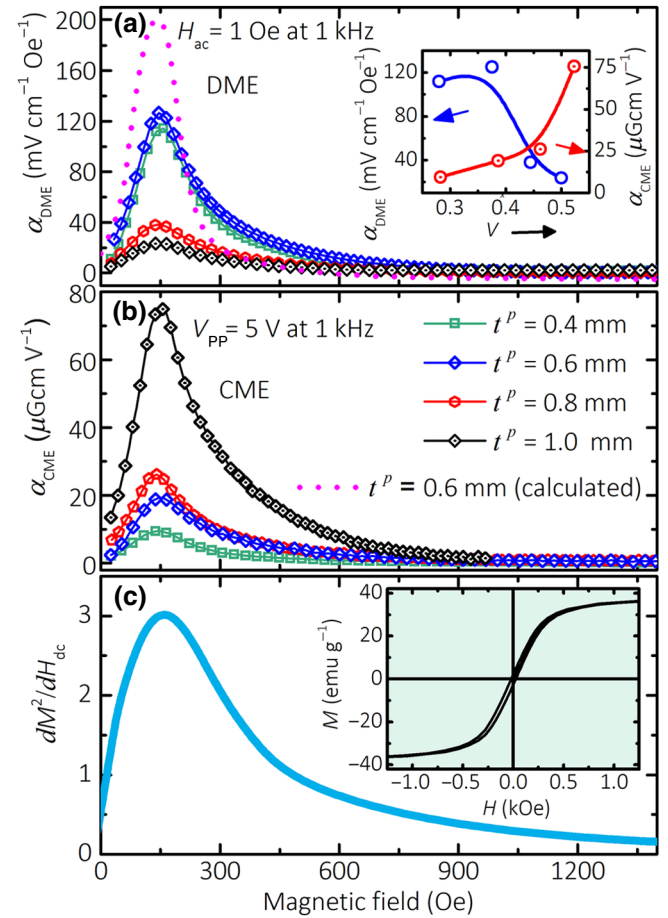


FIG. 5. Variation of (a) α_{DME} and (b) α_{CME} as a function of dc magnetic field for laminate composites with $t^p = 0.4, 0.6, 0.8,$ and 1.0 mm. Inset in (a) shows maximum values of α_{DME} and α_{CME} as a function of BZT-BCT volume fraction, V . (c) Plot of dM^2/dH_{dc} with respect to external H_{dc} ; inset shows the M - H curve of the NFO sample. Calculated α_{DME} value for $t^p = 0.6$ mm is plotted along with measured α_{DME} values.

of maximum α_{DME} and α_{CME} with respect to the bilayer volume fraction are drawn in the inset of Fig. 5(a), which shows similar behavior to that reported for bilayer structures [10,26]. To address the effect of ac field amplitude, if any, the ME output voltage and coupling coefficients are recorded as a function of ac magnetic field at constant dc magnetic field in both increasing and decreasing directions. For this purpose, the composite with $t^p = 0.8$ mm is considered as a reference, and the obtained data are plotted in Fig. S1 within the Supplemental Material [37]. Figure S1 reveals the linear variation of the ME voltage output and subtle change in α_{DME} with ac magnetic field amplitude without a hysteretic character. These features strongly suggest that the ac field amplitude has a negligible effect on the dc field in measurements.

It is expected that ME coupling should show a linear relation with the derivative of the square of the magnetization (dM^2/dH_{dc}) versus the magnetic field [38], which is plotted in Fig. 5(c) for the NFO sample (the corresponding M versus H curve of the NFO sample is shown in the inset). Figure 5(c) reveals that the field-dependent ME coefficients mimic the dM^2/dH_{dc} versus H_{dc} behavior of the NFO sample. The hysteresis behavior of α_{DME} and α_{CME} , as confirmed by measuring the increment and decrement cycles of H_{dc} , for all samples is shown in Fig. S2 (left panel) and Fig. S2 (right panel), respectively, within the Supplemental Material [37].

To probe the strain-transfer efficiency across the bilayer, we calculate transverse α_{DME} as a function of the dc magnetic field [10,14,39]:

$$\alpha_{\text{DME}} = \frac{-2k_p d_{31}^p t^m}{(s_{11}^m + s_{12}^m) \varepsilon_{33}^p k_p t^p + (s_{11}^p + s_{12}^p) \varepsilon_{33}^p t^m - 2(d_{31}^p)^2 k_p t^m} \times \frac{d\lambda}{dH_{\text{dc}}}, \quad (4)$$

where s_{ij}^p and s_{ij}^m are the elastic compliance coefficients for the piezoelectric phase (for BZT-BCT, $s_{11}^p = 13.6 \times 10^{-12} \text{ m}^2 \text{ N}^{-1}$; $s_{12}^p = -5.32 \times 10^{-12} \text{ m}^2 \text{ N}^{-1}$) and the magnetostrictive phase (for NFO, $s_{11}^m = 6.5 \times 10^{-12} \text{ m}^2 \text{ N}^{-1}$; $s_{12}^m = -2.4 \times 10^{-12} \text{ m}^2 \text{ N}^{-1}$), respectively, and d_{31}^p is the relative piezoelectric coefficient (for BZT-BCT, $d_{31}^p = -185 \text{ pC N}^{-1}$). These values are inferred from the literature [12,40]. ε_{33}^p is the relative dielectric coefficient of the piezoelectric phase. For BZT-BCT, the measured value is $\varepsilon_{33}^p = 2690\varepsilon_0$, where ε_0 is the absolute permittivity and k_p for the BZT-BCT compound is 0.41. The measured magnetostriction (λ) versus H_{dc} for the NFO sample is shown in Fig. S3 within the Supplemental Material [37]. The calculated value of α_{DME} from Eq. (4) as a function of the H_{dc} field is plotted for a particular thickness of $t^p = 0.6$ mm along with the observed values in Fig. 5(a). It is observed that the calculated value of α_{DME} follows a similar trend to that of experimentally measured values, with respect

to the dc bias field, but with slightly larger α_{DME} values. Notably, the calculated α_{DME} value is higher due to the assumption of 100% strain transfer at the interface and the approximation used in the calculation. A comparison between the calculated and observed α_{DME} values reveals that the strain-transfer efficiency for the BZT-BCT/NFO bilayer composite is about 63%. This suggests the existence of effective bonding between the piezoelectric and piezomagnetic layers.

F. Resonance magnetoelectric effect

For the resonance study, initially, frequency-dependent ME measurements are carried out without (self-bias) and with an external bias field of 145 Oe for all composites. The bias field of 145 Oe is chosen because it is where both α_{DME} and α_{CME} show maximum values at 1 kHz. The frequency response of α_{DME} and α_{CME} measured under 50–300 kHz self-bias and bias-field conditions for the $t^p = 0.4$ mm laminate composite, along with their impedance data, are plotted in Fig. 6.

The maximum values of α_{DME} and α_{CME} under self-bias conditions are observed at f_R mode and they are $2 \text{ V cm}^{-1} \text{ Oe}^{-1}$ at 315.24 kHz and 2 mGcm V^{-1} at

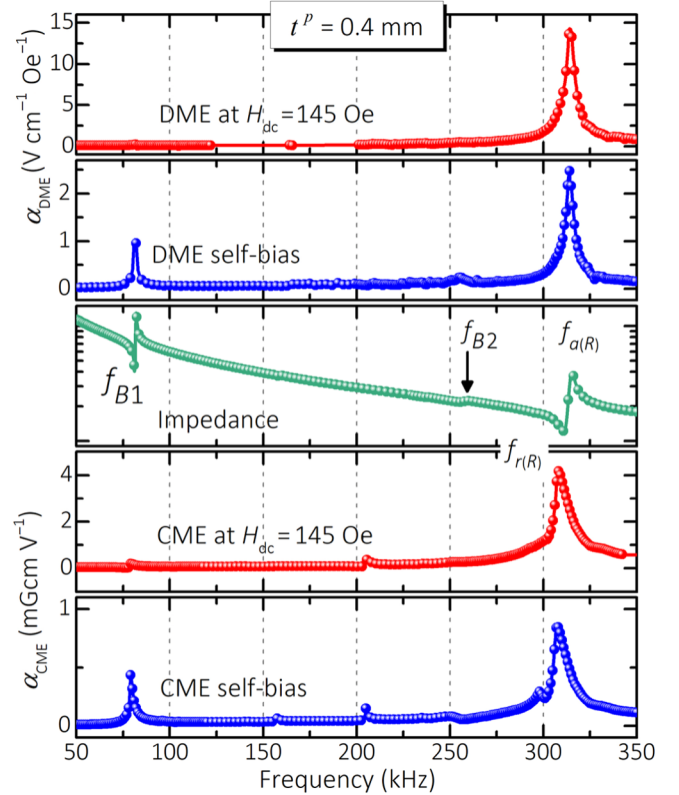


FIG. 6. α_{DME} and α_{CME} plots as a function of frequencies under self-bias and bias conditions, along with impedance, for $t^p = 0.4$ mm laminate composites.

TABLE I. Obtained ME coupling coefficients at off-resonance and resonance frequencies for different thicknesses of BZT-BCT under self-bias and bias-field conditions.

t^p (mm)	α_{DME} (V cm ⁻¹ Oe ⁻¹)				α_{CME} (mGcm V ⁻¹)			
	Self-bias		At 145 Oe		Self-bias		At 145 Oe	
	f_{B1}	f_R	f_{B1}	f_R	f_{B1}	f_R	f_{B1}	f_R
0.4	0.99	2.50	0.30	13.99	0.45	0.85	0.31	4.21
0.6	1.70	1.70	3.00	8.14	2.10	2.26	1.58	11.22
0.8	2.92	3.56	8.18	22.50	0.91	6.12	2.88	25.15
1.0	1.09	3.66	4.80	13.29	1.65	3.72	7.75	16.41

311.26 kHz, respectively, as observed in Fig. 6. However, the corresponding values observed under a bias field of 145 Oe are enhanced to 13.99 V cm⁻¹ Oe⁻¹ and 4.21 mGcm V⁻¹. The above observation suggests that the measurements under bias field augment elastic vibration in the sample and thereby result in the observed large enhancement in ME coupling coefficients. Similarly, at f_{B1} , the maximum values of α_{DME} and α_{CME} are 0.3 V cm⁻¹ Oe⁻¹ at 82.10 kHz and 0.31 mGcm V⁻¹ at 81.18 kHz, respectively, under bias-field conditions. Notably, the frequencies at which α_{DME} and α_{CME} show maximum values match those of f_a and f_r , respectively, for all resonance modes of the bilayer structure, which is in agreement with Ref. [29]. Similarly, the measured α_{DME} and α_{CME} values for the composites with $t^p = 0.6, 0.8,$ and 1.0 mm are plotted in Figs. S4(a)–S4(c) within the Supplemental Material [37], respectively. For comparison, the observed coupling coefficients of all composite samples are tabulated in Table I. From Table I, it is inferred that the ME coupling coefficients show maximum values for the composite with $t^p = 0.8$ mm at f_R , and it is 100% larger than that of the $t^p = 0.6$ mm laminate composites.

G. Effect of resonance-mode tuning on the magnetoelectric effect

The observed highest ME coupling coefficients at f_R for the composite with $t^p = 0.8$ mm is due to the superimposition of bending and radial acoustic modes. To elucidate this further, the frequency response of the phase of

the impedance spectrum, α_{DME} , and α_{CME} are plotted in Figs. 7(a)–7(c), respectively, for composites with $t^p = 0.4, 0.6, 0.8,$ and 1.0 mm. Figure 7(a) reveals a systematic shift in the phases of the bending and radial modes with variation in t^p and their in-phase superimposition for the $t^p = 0.8$ mm sample at around 295 kHz. Accordingly, the phase-matched laminate structure with $t^p = 0.8$ mm, where f_{B2} and f_R are in-phase superimposed, leads to a remarkable mechanical vibration, in comparison to that of its natural radial and bending modes. Hence, the $t^p = 0.8$ mm composite shows a larger α_{DME} of 22.5 V cm⁻¹ Oe⁻¹ and an α_{CME} value of 25 mGcm V⁻¹ at 301 kHz than those of the other composites, $t^p = 0.4, 0.6,$ and 1.0 mm, as shown in Figs. 7(b) and 7(c).

To further confirm the observed enhancement in the ME effect, measurements of α_{DME} and α_{CME} are carried out at the radial-mode resonance frequency as a function of H_{dc} . The respective results are shown in Fig. S5 (left panel) and Fig. S5 (right panel) within the Supplemental Material for all four composite structures [37]. The plots show typical behavior of the ME coupling coefficient as a function of H_{dc} , with their peak values matching well with the observed α_{DME} and α_{CME} values from the resonance measurements [as shown in Figs. 7(b) and 7(c)].

The observed effect of volume fraction on the ME effect can be verified from the following calculation based on the theoretical model [25,26]. The transverse ME coupling coefficient for a bilayer disk-shaped laminate composite under the resonance conditions can be calculated from [25]

$$\alpha_{\text{DME}} = \frac{(1+v)(1-V)s_{11}^p J_1(kR) d_{31}^p (q_{11}^m + q_{12}^m) \mu_{\text{eff}}}{(1-v)s_{11}^p [aJ_0(kR) - (1-v)s_1 J_1(kR)] \varepsilon_{33}^p + 2[aJ_0(kR) - s_3 J_1(kR)] (d_{31}^p)^2}, \quad (5)$$

where $k = \omega \sqrt{\rho \{V/[s_{11}^p(1-v_p^2)] + (1-V)/[s_{11}^m(1-v_m^2)]\}^{-1}}$, $a = kRs_1$, $s_1 = [Vs_{11}^m + (1-V)s_{11}^p]$, $s_3 = (1-v)(1-V)s_{11}^p + 2Vs_{11}^m$, and $J_n(kR)$ is the Bessel's function. q_{ij}^m are the piezomagnetic coefficients of the magnetostrictive phase (for NFO, $q_{11}^m = -680 \times 10^{-12}$ m A⁻¹; $q_{12}^m =$

125×10^{-12} m A⁻¹) [25]. μ_{eff} is the effective permeability coefficient of the magnetostrictive phase. v_m and v_p are the Poisson ratio of the magnetostrictive and piezoelectric phases, respectively, and for simplicity we consider $v_m = v_p = v = -s_{12}^m/s_{11}^m = 0.36$ [28]. The α_{DME} calculations

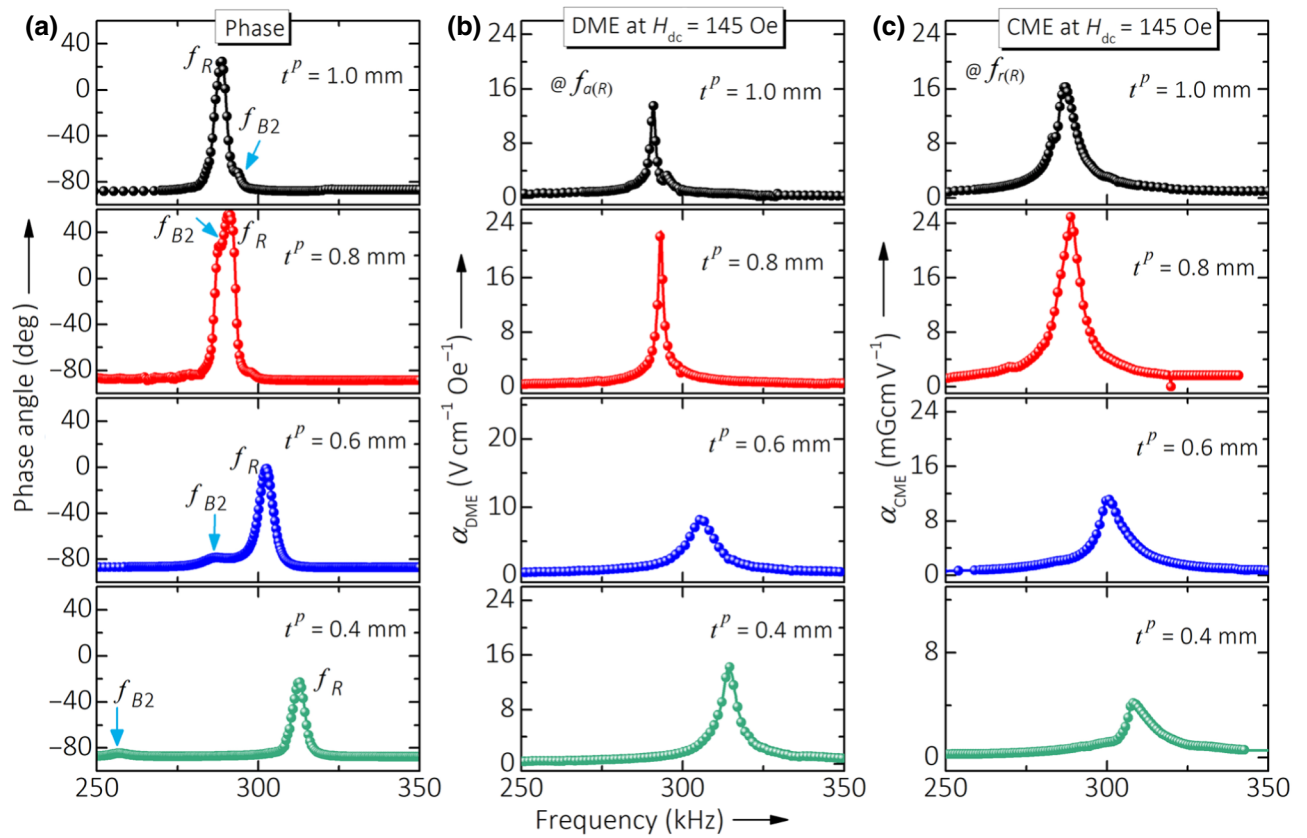


FIG. 7. (a) Phase of vibration, (b) α_{DME} at bias field, and (c) α_{CME} at bias field for BZT-BCT/NFO bilayer laminate composites with various t^P at acoustic modes of the f_R and f_{B2} frequency range.

are performed for different volume fractions using the above parameters in Eq. (5), and the calculated values as a function of frequency at various V are plotted in Fig. S6 within the Supplemental Material [37]. To corroborate the effect of volume fraction on ME coupling, the observed and calculated resonance frequencies are shown in Fig. 8(a). The corresponding observed and calculated α_{DME} values are given in Fig. 8(b). The calculated volume-fraction-dependent α_{DME} follows a similar trend to that of the observed values and displays maximum ME coupling at the frequency where both radial and bending modes exhibit in-phase superimposition. Notably, the systematic decrease in calculated resonance frequency (frequency where the calculated α_{DME} is maximum) with V is similar to the observed trend displayed by the radial mode, as shown in Fig. 8(a). Overall, these results reveal agreement between the experimental and theoretical data.

H. Magnetic energy harvesting in the resonance-mode-engineered bilayer laminate composite

Therefore, the bilayer laminate composite with an optimized t^P of 0.8 mm, showing enhanced ME coupling coefficients, can generate a large electric voltage from a

low magnetic field, and hence, can be employed for energy harvesting applications. For the energy harvesting characteristics of the ME bilayer laminate composite, initially, the output voltage due to the DME effect is measured in the $t^P = 0.8$ mm bilayer composite by exciting the sample with a H_{ac} of 10 Oe at 295 kHz, where f_{B2} and f_R are superimposed. The α_{DME} measured under the self-bias condition at 295 kHz gives a peak-to-peak electrical ac output voltage of 4 V, as displayed in Fig. 9(a). In addition to the self-bias effect, the α_{DME} is recorded under a low dc bias field of 145 Oe (where the maximum ME coefficient is observed for the composite). The measurement shows a large ac output peak-to-peak voltage of 16 V across the sample, as shown in Fig. 9(b). The observed enhancement in output voltage is the consequence of DME coupling in the composite, with larger mechanical oscillation in the structure caused by the superimposition of f_{B2} and f_R at 295 kHz. The demonstrated significantly larger electrical output voltage at a low H_{dc} field suggests that the BZT-BCT-based laminate composite is suitable for magnetic energy harvesting.

To demonstrate energy harvesting, the output ac signal from the composite measured at 295 kHz under the H_{dc} of 145 Oe is converted into a dc electrical signal by a bridge rectifier, as shown in Fig. 9(c) [2–4]. The rectified dc

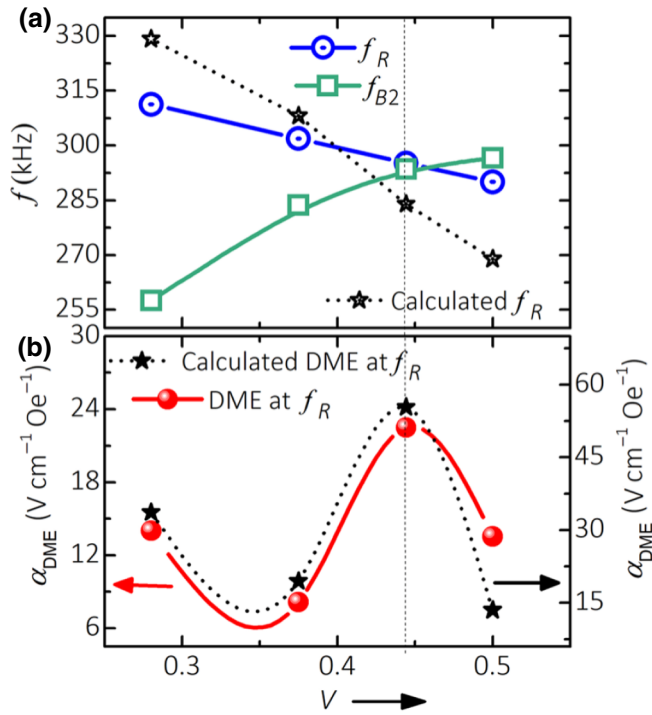


FIG. 8. Observed and calculated (a) electromechanical resonance frequencies and (b) α_{DME} of different bilayers samples plotted as a function of volume fraction, V .

voltage and current of the bilayer measured as a function of different load resistors in the circuit are plotted in Fig. 9(d). The plot suggests that the dc voltage varies from 3 to 16 V for variation of the load resistance from 1 k Ω to 10 M Ω ; the corresponding current varies from 7.5 mA to 20 nA. The calculated power density as a function of load resistance displays a maximum value of about 1.5 mW cm $^{-2}$ at 10 k Ω load resistance, as shown in Fig. 9(e). The observed large power density in the bilayer laminate composite illustrates the efficiency of magnetic energy harvesting for magnetic sensor applications. This is verified by powering a series of LEDs through the output of the rectifier circuit connected to the bilayer composite structure. The photograph of glowing LEDs is shown in the inset of Fig. 9(e). Therefore, the demonstration of energy harvesting from the high-frequency source is suitable to power various wireless communicating electronic devices in the presence of a magnetic field. Additionally, the proposed mechanism can also be envisaged to harvest energy from sources operating in the low-frequency range. For example, tuning of the resonance mode towards low frequency could be achieved by choosing an appropriate configuration of the ME composites, such as rectangular bilayers, multilayers, and cantilever geometries [3–5,12,41,42].

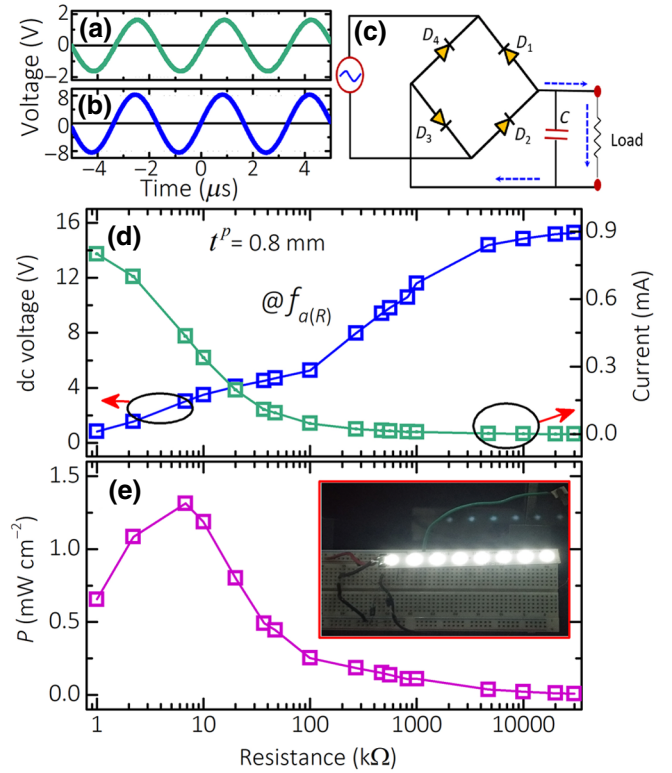


FIG. 9. Recorded output ac voltage from DME measurements at (a) zero bias and (b) 145 Oe bias field for $t^p = 0.8$ mm bilayer laminate composite. (c) Schematic diagram of the bridge rectifier used to convert output ac voltage into dc voltage. Demonstration of magnetic energy harvesting: (d) observed dc voltage and its current obtained after rectification and (e) calculated power with respect to different resistors. Inset shows an energy harvesting experiment by lighting a series of LEDs powered by the obtained output voltage from the ME laminate composite at a bias field of 145 Oe.

IV. CONCLUSIONS

The disk-shaped bilayer laminate composite structure prepared by bonding piezoelectric BZT-BCT and piezomagnetic NFO compounds reveals several acoustic resonance modes in their frequency-dependent impedance measurements. The strain-mediated ME coupling between piezoelectric and piezomagnetic phases is performed on the BZT-BCT/NFO laminate composites, with the thickness of the BZT-BCT layer being 0.4, 0.6, 0.8, and 1.0 mm, by keeping the NFO thickness constant at 1 mm. The off-resonance ME measurements reveal the highest α_{DME} of 124 mV cm $^{-1}$ Oe $^{-1}$ for the 0.6BZT-BCT/NFO sample and the highest α_{CME} of 78 μ Gcm V $^{-1}$ for the 1.0BZT-BCT/NFO sample at 1 kHz frequency. The calculated α_{DME} , in comparison with the observed value, suggests 63% strain transfer efficiency across the bilayers. It is proposed to engineer the second bending mode to superimpose with the radial mode by varying the bilayer disk thickness for enhanced ME coupling. As

proposed, the composite indeed reveals large ME coupling coefficients at the thickness where the modes are superimposed. Notably, the in-phase superimposition of electromechanical modes and the effective strain transfer efficiency across the bilayer lead to maximum ME coefficients of $\alpha_{\text{DME}} = 22.5 \text{ V cm}^{-1} \text{ Oe}^{-1}$ and $\alpha_{\text{CME}} = 25.14 \text{ mG cm V}^{-1}$, which are 100% larger than the values observed when the modes are well separated. Subsequent calculations carried out based on the theoretical model validate the experimentally observed results. The potential of the ME effect in the bilayer composite is demonstrated by powering a series of LEDs in a magnetic energy harvesting experiment. Although the ambient frequencies of most of the environmental energy sources are at the low-frequency range, the presented energy harvesting in the ME composite from the magnetic source suggests its potential application in relevant wireless powering of small devices in the high-frequency range. The proposed idea of tuning of the resonance modes opens up a way to design a better ME composite with superior ME coupling.

ACKNOWLEDGMENTS

The authors acknowledge the Physics Department's magnetic measurement facility sponsored by the DST-FIST program.

- [1] D. Maurya, M. Peddigari, M.-G. Kang, L. D. Geng, N. Sharpes, V. Annapureddy, H. Palneedi, R. Sriramdas, Y. Yan, H.-C. Song, Y. U. Wang, J. Ryu, and S. Priya, Lead-free piezoelectric materials and composites for high power density energy harvesting, *J. Mater. Res.* **33**, 2235 (2018).
- [2] C. Baek, J. H. Yun, J. E. Wang, C. K. Jeong, K. J. Lee, K. Il Park, and D. K. Kim, A flexible energy harvester based on a lead-free and piezoelectric BCTZ nanoparticle-polymer composite, *Nanoscale* **8**, 17632 (2016).
- [3] V. Annapureddy, H. Palneedi, G.-T. Hwang, M. Peddigari, D.-Y. Jeong, W.-H. Yoon, K.-H. Kim, and J. Ryu, Magnetic energy harvesting with magnetoelectrics: An emerging technology for self-powered autonomous systems, *Sustain. Energy Fuels* **1**, 2039 (2017).
- [4] V. Annapureddy, S. M. Na, G. T. Hwang, M. G. Kang, R. Sriramdas, H. Palneedi, W. H. Yoon, B. D. Hahn, J. W. Kim, C. W. Ahn, D. S. Park, J. J. Choi, D. Y. Jeong, A. B. Flatau, M. Peddigari, S. Priya, K. H. Kim, and J. Ryu, Exceeding milli-watt powering magneto-mechano-electric generator for standalone-powered electronics, *Energy Environ. Sci.* **11**, 818 (2018).
- [5] V. Annapureddy, H. Y. Lee, W. H. Yoon, H. J. Woo, J. H. Lee, H. Palneedi, H. J. Kim, J. J. Choi, D. Y. Jeong, S. N. Yi, and J. Ryu, Enhanced magnetic energy harvesting properties of magneto-mechano-electric generator by tailored geometry, *Appl. Phys. Lett.* **109**, 093901 (2016).
- [6] S. Ju, S. H. Chae, Y. Choi, S. Lee, H. W. Lee, and C.-H. Ji, A low frequency vibration energy harvester using magnetolectric laminate composite, *Smart Mater. Struct.* **22**, 115037 (2013).
- [7] Z. Hu, J. Qiu, X. Wang, Y. Gao, X. Liu, Q. Chang, Y. Long, and X. He, An integrated multi-source energy harvester based on vibration and magnetic field energy, *AIP Adv.* **8**, 056623 (2018).
- [8] M. P. Aparicio, A. Bakkali, J. P. Sebastia, T. Sogorb, V. Llario, and A. Bou, Radio Frequency Energy harvesting-sources and techniques, *Intech i*, 13 (2016).
- [9] A. Nechibvute, A. Chawand, N. Taruvinga, and P. Luhanga, Radio frequency energy harvesting sources, *Acta Electrotech. Inform.* **4**, 19 (2017).
- [10] G. Srinivasan, Magnetolectric composites, *Annu. Rev. Mater. Res.* **40**, 153 (2010).
- [11] J. Ma, J. Hu, Z. Li, and C. W. Nan, Recent progress in multiferroic magnetolectric composites: From bulk to thin films, *Adv. Mater.* **23**, 1062 (2011).
- [12] Z. Chu, M. Pourhosseiniasl, and S. Dong, Review of multilayered magnetolectric composite materials and devices applications, *J. Phys. D: Appl. Phys.* **51**, 243001 (2018).
- [13] M. Feng, J. J. Wang, J. M. Hu, J. Wang, J. Ma, H. B. Li, Y. Shen, Y. H. Lin, L. Q. Chen, and C. W. Nan, Optimizing direct magnetolectric coupling in Pb(Zr, Ti)O₃/Ni multiferroic film heterostructures, *Appl. Phys. Lett.* **106**, 072901 (2015).
- [14] G. Srinivasan, E. T. Rasmussen, J. Gallegos, R. Srinivasan, Y. I. Bokhan, and V. M. Laletin, Magnetolectric bilayer and multilayer structures of magnetostrictive and piezoelectric oxides, *Phys. Rev. B* **64**, 214408 (2001).
- [15] G. T. Hwang, H. Palneedi, B. M. Jung, S. J. Kwon, M. Peddigari, Y. Min, J. W. Kim, C. W. Ahn, J. J. Choi, B. D. Hahn, J. H. Choi, W. H. Yoon, D. S. Park, S. B. Lee, Y. Choe, K. H. Kim, and J. Ryu, Enhancement of magneto-electric conversion achieved by optimization of interfacial adhesion layer in laminate composites, *ACS Appl. Mater. Interfaces* **10**, 32323 (2018).
- [16] A. B. Swain, M. Rath, S. Dinesh Kumar, M. S. Ramachandra Rao, V. Subramanian, and P. Murugavel, Large magnetolectric coupling in 0.5Ba(Zr_{0.2}Ti_{0.8})O₃-0.5(Ba_{0.7}Ca_{0.3})TiO₃ film on Ni foil, *J. Phys. D: Appl. Phys.* **52**, 065004 (2019).
- [17] H. Palneedi, D. Maurya, Gi-Y. Kim, S. Priya, S. J. Joong, L. Kang, K. H. Kim, S. Y. Choi, and J. Ryu, Enhanced off-resonance magnetolectric response in laser annealed PZT thick film grown on magnetostrictive amorphous metal substrate, *Appl. Phys. Lett.* **107**, 012904 (2015).
- [18] G. Srinivasan, E. T. Rasmussen, B. J. Levin, and R. Hayes, Magnetolectric effect in bilayer and multilayer structures of magnetostrictive and piezoelectric perovskite oxides, *Phys. Rev. B* **65**, 134402 (2002).
- [19] G. Srinivasan, E. T. Rasmussen, and R. Hayes, Magnetolectric effect in ferrite-lead zirconate titanate layered composites: The influence of zinc substitution in ferrites, *Phys. Rev. B* **67**, 014418 (2003).
- [20] Y. J. Zhang, J. H. Chen, L. L. Li, J. Ma, C. W. Nan, and Y. H. Lin, Ferroelectric strain modulation of antiferromagnetic moments in Ni/NiO ferromagnet/antiferromagnet heterostructures, *Phys. Rev. B* **95**, 174420 (2017).
- [21] H. Palneedi, D. Maurya, L. D. Geng, H. C. Song, G. T. Hwang, M. Peddigari, V. Annapureddy, K. Song, Y. S. Oh, S. C. Yang, Y. U. Wang, S. Priya, and J. Ryu,

- Enhanced self-biased magnetoelectric coupling in laser-annealed $\text{Pb}(\text{Zr}, \text{Ti})\text{O}_3$ thick film deposited on Ni foil, *ACS Appl. Mater. Interfaces* **10**, 11018 (2018).
- [22] H. Palneedi, H. G. Yeo, G.-T. Hwang, V. Annapureddy, J.-W. Kim, J.-J. Choi, S. T. McKinstry, and J. Ryu, A flexible, high-performance magnetoelectric heterostructure of (001) oriented $\text{Pb}(\text{Zr}_{0.52}\text{Ti}_{0.48})\text{O}_3$ film grown on Ni foil, *APL Mater.* **5**, 096111 (2017).
- [23] H. Palneedi, V. Annapureddy, H. Y. Lee, J. J. Choi, S. Y. Choi, S. Y. Chung, S. J. L. Kang, and J. Ryu, Strong and anisotropic magnetoelectricity in composites of magnetostrictive Ni and solid-state grown lead-free piezoelectric, BZT–BCT single crystals, *J. Asian Ceram. Soc.* **5**, 36 (2017).
- [24] D. A. Filippov, Theory of the magnetoelectric effect in ferromagnetic-piezoelectric heterostructure, *Phys. Solid State* **47**, 1118 (2005).
- [25] M. I. Bichurin, V. M. Petrov, S. V. Averkin, and A. V. Filippov, Electromechanical resonance in magnetoelectric layered structures, *Phys. Solid State* **52**, 2116 (2010).
- [26] M. I. Bichurin, D. A. Filippov, V. M. Petrov, V. M. Laletsin, N. Paddubnaya, and G. Srinivasan, Resonance magnetoelectric effects in layered magnetostrictive-piezoelectric composites, *Phys. Rev. B* **68**, 132408 (2003).
- [27] D. V. Chashin, Y. K. Fetisov, K. E. Kamentsev, and G. Srinivasan, Resonance magnetoelectric interactions due to bending modes in a nickel-lead zirconate titanate bilayer, *Appl. Phys. Lett.* **92**, 102511 (2008).
- [28] S. Dinesh Kumar, G. Ramesh, and V. Subramanian, Enhanced self-biased direct and converse magnetoelectric effect in $\text{Pb}(\text{In}_{1/2}\text{Nb}_{1/2})\text{O}_3 - \text{PbTiO}_3/\text{NiFe}_2\text{O}_4$ bi-layer laminate composite, *J. Mater. Sci: Mater Electron.* **26**, 2682 (2015).
- [29] K. H. Cho and S. Priya, Direct and converse effect in magnetoelectric laminate composites, *Appl. Phys. Lett.* **98**, 232904 (2011).
- [30] H. Palneedi, S.-M. Na, G.-T. Hwang, M. Peddigari, K. Woo Shin, K. H. Kim, and J. Ryu, Highly tunable magnetoelectric response in dimensional gradient laminate composites of Fe-Ga alloy and $\text{Pb}(\text{Mg}_{1/3}\text{Nb}_{2/3})\text{O}_3$ - $\text{Pb}(\text{Zr}, \text{Ti})\text{O}_3$ single crystal, *J. Alloy Compd.* **765**, 764 (2018).
- [31] W. Liu and X. Ren, Large Piezoelectric Effect in Pb-Free Ceramics Wenfeng, *Phys. Rev. Lett.* **103**, 257602 (2009).
- [32] A. B. Swain, V. Subramanian, and P. Murugavel, The role of precursors on piezoelectric and ferroelectric characteristics of 0.5BCT-0.5BZT ceramic, *Ceram. Int.* **44**, 6861 (2018).
- [33] M. Guo, S. Dong, B. Ren, and H. Luo, A double-mode piezoelectric single-crystal ultrasonic micro-actuator, *IEEE Trans. Ultrason. Ferroelectr. Freq. Control* **57**, 2596 (2010).
- [34] S. Dinesh Kumar, J. Magesh, and V. Subramanian, Tuning of bandwidth by superposition of bending and radial resonance modes in bilayer laminate composite, *Mater. Des.* **122**, 315 (2017).
- [35] A. Srinivas, R. V. Krishnaiah, V. L. Niranjani, S. V. Kamat, T. Karthik, and S. Asthana, Ferroelectric, piezoelectric and mechanical properties in lead free $(0.5)\text{Ba}(\text{Zr}_{0.2}\text{Ti}_{0.8})\text{O}_3$ - $(0.5)(\text{Ba}_{0.7}\text{Ca}_{0.3})\text{TiO}_3$ electroceramics, *Ceram. Int.* **41**, 1980 (2015).
- [36] A. K. S. Molakeri, S. Kalyane, A. B. Kulkarni, and S. N. Mathad, Elastic properties of nickel ferrite synthesized by combustion and microwave method using FT-IR spectra, *Int. J. Adv. Sci. Eng.* **3**, 422 (2017).
- [37] See the Supplemental Material at <http://link.aps.org/supplemental/10.1103/PhysRevApplied.13.024026> for ME output voltage and α_{DME} as a function of H_{ac} ; α_{DME} and α_{CME} as a function of H_{dc} ; the magnetostriction data of NFO; α_{DME} and α_{CME} as a function of frequency for various f^{p} ; α_{DME} and α_{CME} as a function of H_{dc} ; and calculated α_{DME} as a function of frequency.
- [38] C. S. Park, A. Khachaturyan, and S. Priya, Giant magnetoelectric coupling in laminate thin film structure grown on magnetostrictive substrate, *Appl. Phys. Lett.* **100**, 192904 (2012).
- [39] M. I. Bichurin, V. M. Petrov, and G. Srinivasan, Theory of low-frequency magnetoelectric coupling in magnetostrictive-piezoelectric bilayers, *Phys. Rev. B* **68**, 054402 (2003).
- [40] D. A. Tuan, N. T. Tinh, V. T. Tung, and T. V. Chuong, Ferroelectric and piezoelectric properties of Lead-Free BCT-xBZT solid solutions, *Mater. Trans.* **56**, 1370 (2015).
- [41] B. Deka, Y.-W. Lee, I.-R. Yoo, D.-W. Gwak, J. Cho, H.-C. Song, J.-J. Choi, B.-D. Hahn, C.-W. Ahn, and K.-H. Cho, Designing ferroelectric/ferromagnetic composite with giant self-biased magnetoelectric effect, *Appl. Phys. Lett.* **115**, 192901 (2019).
- [42] M. G. Kang, R. Sriramdas, H. Lee, J. Chun, D. Maurya, G. T. Hwang, J. Ryu, and S. Priya, High power magnetic field energy harvesting through amplified magneto-mechanical vibration, *Adv. Energy Mater.* **8**, 1703313 (2018).